AIP | Journal of Applied Physics

Deposition and characterization of B4C/CeO2 multilayers at 6.x nm extreme ultraviolet wavelengths

M. G. Sertsu, A. Giglia, S. Brose, D. Park, Z. S. Wang, J. Mayer, L. Juschkin, and P. Nicolosi

Citation: Journal of Applied Physics **119**, 095301 (2016); doi: 10.1063/1.4942656
View online: http://dx.doi.org/10.1063/1.4942656
View Table of Contents: http://scitation.aip.org/content/aip/journal/jap/119/9?ver=pdfcov
Published by the AIP Publishing

Articles you may be interested in

Interlayer growth in Mo/B4C multilayered structures upon thermal annealing
J. Appl. Phys. **113**, 144310 (2013); 10.1063/1.4800910

Ion assisted growth of B4C diffusion barrier layers in Mo/Si multilayered structures
J. Appl. Phys. **111**, 064303 (2012); 10.1063/1.3693992

Ferroelectric properties of Bi 4 − x Ce x Ti 3 O 12 (0 x 4) thin film array fabricated from Bi 2 O 3/Ce O 2/Ti O 2 multilayers using multitarget sputtering
Appl. Phys. Lett. **92**, 052911 (2008); 10.1063/1.2841039

Effect of interface treatment with assisted ion beam on Mo-Si multilayer formation for mask blanks for extreme ultraviolet lithography
J. Vac. Sci. Technol. B **25**, 1554 (2007); 10.1116/1.2768604

Thermal stability of 2.4 nm period Ni–Nb/C multilayer x-ray mirror
Appl. Phys. Lett. **77**, 3654 (2000); 10.1063/1.1328761

Reuse of AIP Publishing content is subject to the terms at: https://publishing.aip.org/authors/rights-and-permissions. IP: 147.162.2.240 On: Tue, 01 Mar 2016 15:38:42

JOURNAL OF APPLIED PHYSICS 119, 095301 (2016)

Deposition and characterization of B_4C/CeO_2 multilayers at 6.x nm extreme ultraviolet wavelengths

M. G. Sertsu,[1,2,3,a)] A. Giglia,[4] S. Brose,[5] D. Park,[6] Z. S. Wang,[7] J. Mayer,[6] L. Juschkin,[3,8] and P. Nicolosi[1,2]

[1]*Department of Information Engineering, University of Padova, via Gradenigo 6B, 35131 Padova, Italy*
[2]*CNR—IFN UOS Padova, Via Trasea 7, 35131 Padova, Italy*
[3]*Experimental Physics of EUV, JARA-FIT, RWTH Aachen University, Steinbachstr. 15, 52074 Aachen, Germany*
[4]*CNR- Istituto Officina Materiali, I-34149 Trieste, Italy*
[5]*Chair for the Technology of Optical Systems (TOS), JARA-FIT, RWTH Aachen University, Steinbachstr. 15, 52074 Aachen, Germany*
[6]*Central Facility for Electron Microscopy (GFE), JARA-FIT, RWTH Aachen University, Ahornstr. 55, D-52074 Aachen, Germany*
[7]*Institute of Precision Optics Engineering, Tongji University, Shanghai 200092, China*
[8]*Peter Grünberg Institut (PGI-9), JARA-FIT, Forschungszentrum Jülich GmbH, 52425 Jülich, Germany*

(Received 11 December 2015; accepted 11 February 2016; published online 1 March 2016)

New multilayers of boron carbide/cerium dioxide (B_4C/CeO_2) combination on silicon (Si) substrate are manufactured to represent reflective-optics candidates for future lithography at 6.x nm wavelength. This is one of only a few attempts to make multilayers of this kind. Combination of several innovative experiments enables detailed study of optical properties, structural properties, and interface profiles of the multilayers in order to open up a room for further optimization of the manufacturing process. The interface profile is visualized by high-angle annular dark-field imaging which provides highly sensitive contrast to atomic number. Synchrotron based at-wavelength extreme ultraviolet (EUV) reflectance measurements near the boron (B) absorption edge allow derivation of optical parameters with high sensitivity to local atom interactions. X-ray reflectivity measurements at Cu-K_{alpha} (8 keV) determine the period of multilayers with high in-depth resolution. By combining these measurements and choosing robust nonlinear curve fitting algorithms, accuracy of the results has been significantly improved. It also enables a comprehensive characterization of multilayers. Interface diffusion is determined to be a major cause for the low reflectivity performance. Optical constants of B_4C and CeO_2 layers are derived in EUV wavelengths. Besides, optical properties and asymmetric thicknesses of inter-diffusion layers (interlayers) in EUV wavelengths near the boron edge are determined. Finally, ideal reflectivity of the B_4C/CeO_2 combination is calculated by using optical constants derived from the proposed measurements in order to evaluate the potentiality of the design. *© 2016 AIP Publishing LLC.*
[http://dx.doi.org/10.1063/1.4942656]

I. INTRODUCTION

Multilayer (ML) coatings are essential for technological advances and fundamental studies of extreme ultraviolet (EUV) and X-rays. The Mo/Si MLs with >70% reflectivity around 13.5 nm EUV wavelength have enabled the semiconductor industry to print 22 nm features and below on Si wafers. To maintain the Moore's law, efforts are underway to print sub 10 nm features on Si wafers by modifying the 13.5 nm EUV lithography (EUVL) architecture to fulfill engineering requirements of future 6.x nm EUVL.[1–3]

The feasibility of 6.x nm EUVL in terms of source design, output power at the intermediate focus (IF), efficiency of collector mirrors, and conversion efficiencies of solid fuel sources (mainly gadolinium and terbium) seems promising.[4,5] One of the requirements that is lagging behind is reflectivity performance of the ML mirrors for the projection optics module. A reflectivity performance $\geq 70\%$ at near normal incidence is required to enable the technology.

Combinations of lanthanum (La) and boron (B) were among the pioneer MLs deposited and tested for high performance reflectance around 6.x nm wavelengths mainly due to their high optical contrasts. The La/B MLs were found to have lower reflectivity performance due to diffusion induced structural changes at the interfaces.[6] Currently, chemical and process techniques to suppress interface diffusions are implemented and better performances are achieved with combinations of LaN/B_4C and La/B_4C MLs.[7,8] La/B_4C multilayer mirrors designed for reflection at an incidence angle of 45° demonstrated 54.4% reflectivity at 6.7 nm wavelength.[9]

Near normal reflectivity of about 36–40% was obtained from MLs of La/B_4C and La/B_9C for different period values.[10] Maximum peak reflectivity of 48.9% from the La/B_4C multilayer at 6.68 nm and 39.2% from La_2O_3/B_4C at the same wavelength was reported by Platonov *et al.*[11] The 6.x nm MLs research has shown a leap recently after Kuznetsov

[a)]sertsu@dei.unipd.it

Reuse of AIP Publishing content is subject to the terms at: https://publishing.aip.org/authors/rights-and-permissions. IP: 147.162.2.240 On: Tue, 01 Mar 2016 15:38:42

et al.[12] reported 64.1% reflectivity at 1.5° off-normal incidence from La/B MLs manufactured in a hybrid thin-film deposition procedure by passivating the La atoms. Others have also used barrier layers to suppress interface-diffusion. Near normal incidence reflectivity of 58.8% was achieved by using carbon as anti-diffusion barrier layer in La/B_4C MLs.[13]

In this paper, we report on manufacturing and on reflectivity performance assessment of new MLs at the 6.x nm wavelength. This new B_4C/CeO_2 ML combination was deposited using magnetron sputtering facility, and a number of tabletop and synchrotron based measurements were carried out. It is found that near normal incidence reflectivity of the mirror at 6.9 nm is lower than predicted theoretically. The difference is a factor of ∼4.4, which is similar to the discrepancy reported also for the first deposited La/B ML for 6.x nm wavelengths.[14]

The causes of low reflectivity performance of the new ML mirrors are identified and reported here using a combination of different measurements. Further details of interface profiles, EUV optical constants near the boron edge, and layer and interlayer thicknesses are determined in order to modify the deposition processes of such MLs for the reflectivity improvement. The complete ML analysis never was easy and accurate with a single measurement technique. Thus, we performed a combination of grazing incidence EUV reflectivity (GI-EUVR) near absorption edge of boron, X-ray reflectivity (XRR) measurements and various types of scanning transmission electron microscopy (STEM) imaging in order to analyze the MLs with improved accuracy. The ultimate reflectivity performance of the discussed kind of ML mirrors at 6.x nm wavelength is calculated using optical constants of B_4C and CeO_2 layers derived from the presented analysis to check the potential of the mirror assuming ideal interface conditions.

II. SAMPLE DESCRIPTION, EXPERIMENTS, AND DATA ANALYSIS

Two B_4C/CeO_2 ML samples (Table I) were deposited in a magnetron sputtering facility that uses RF power for CeO_2 and DC power for the B_4C at the Institute of Precision Optical Engineering (IPOE), Tongji University. The CeO_2 and B_4C layers were grown from solid targets on Si substrate with typical deposition rates of ∼0.03 nm/s and ∼0.04 nm/s, respectively. The deposition took place in high vacuum chambers and at about room temperature since no heat was applied. The use of magnetron facility enables reactive sputtering of CeO_2 layers from cerium (Ce) targets by controlling the flow rate of oxygen (O_2) in future optimizations of the deposition process.

TABLE I. Design parameters of the two multilayers with the following notations: d is the period, N is number of bilayers, and Γ represents the thickness ratio of the absorber layer (i.e., CeO_2 layer) to the period.

ML types	Design parameters
Sample_01: B_4C/CeO_2	$d = 35$ Å, $t_{CeO2} = 16$ Å, $t_{B4C} = 19$ Å, $N = 40$, $\Gamma = 0.457$
Sample_02: B_4C/CeO_2	$d = 200$ Å, $t_{CeO2} = 80$ Å, $t_{B4C} = 120$ Å, $N = 10$, $\Gamma = 0.400$
Substrate	Si

The first sample, sample_01, is designed for reflection around 6.x nm wavelength and incidence angle of 10° from surface normal. The second sample, sample_02, was coated to enable grazing incidence EUV reflectivity measurements near the boron-edge in EUV (∼186 eV) that is a sensitive at-wavelength metrology over wide grazing incidence angles.

Measurements of at-wavelength GI-EUVR were carried out at the BEAR (Bending magnet for Emission, Absorption and Reflectivity) beam line, ELETTRA Synchrotron in Trieste.[15] The stability and reproducibility of the beam energy coupled with high-accuracy control of the beam-line facility operation and measurement process allowed for noise reduction and in turn an increased reliability of data analysis. The XRR measurements were performed at Cu K_α line (∼8 keV) in a $2\theta - \omega$ scan of the X'PERT-PRO diffractometer configuration to determine periods of the MLs with high in-depth resolution due to the short X-ray wavelength. Independent imaging evidences for the ML structures and interface profiles are provided by bright field STEM (BF-STEM) for sample_02 and high angle annular dark field (HAADF) for sample_01. Both imaging experiments were performed at the Helmholtz Nano electronic Facility and Ernst Ruska-Center of the Forschungszentrum Jülich. A combination of all of the above measurements enables to characterize the MLs with high accuracy and reliability.

Numerical reconstruction of ML parameters from reflectivity measurements is an inversion mathematical problem. It is model and algorithm dependent. Information on the software, reflectivity models, and curve fitting algorithms used to reconstruct optical, structural, and interface profiles of B_4C/CeO_2 MLs from the reflectivity curves is provided below.

Reconstruction of ML parameters from both XRR and GI-EUVR data is performed in a computer program called IMD (modeling and analysis of multilayer films)[16] that can be downloaded from http://www.esrf.eu/Instrumentation/software/data-analysis/xop2.3. Both specular and non-specular (diffuse) optical functions can be calculated in IMD. A nonlinear curve fitting to measured reflectivity curves against a goodness of fit parameter chi-square (χ^2) similar to that of Pearson's criterion[17] retrieves almost any parameter of the MLs. A common practice of curve fitting in IMD embraces generation of independent or joint confidence intervals to make sure fit parameter values are laid in the properly derived allowed ranges (confidence intervals) associated with best curve fitting, based on methods given in Refs. 17 and 18. In IMD, confidence intervals are calculated using either Marquardt or Levenberg-Marquardt gradient-expansion algorithms. For the ML considered here, the nonlinear curve fitting in IMD is repeated until the probability of finding fit parameter values in the confidence intervals reaches 90–98%. Therefore, the discrete thickness and optical constants given in tables and figures are determined with 90–98% probability of finding them within the stated confidence intervals.

Parratt's dynamic reflectivity model of MLs and Debye-Waller like error function ($\sim e^{-\frac{q^2\sigma^2}{2}}$) to account interface

Reuse of AIP Publishing content is subject to the terms at: https://publishing.aip.org/authors/rights-and-permissions. IP: 147.162.2.240 On: Tue, 01 Mar 2016 15:38:42

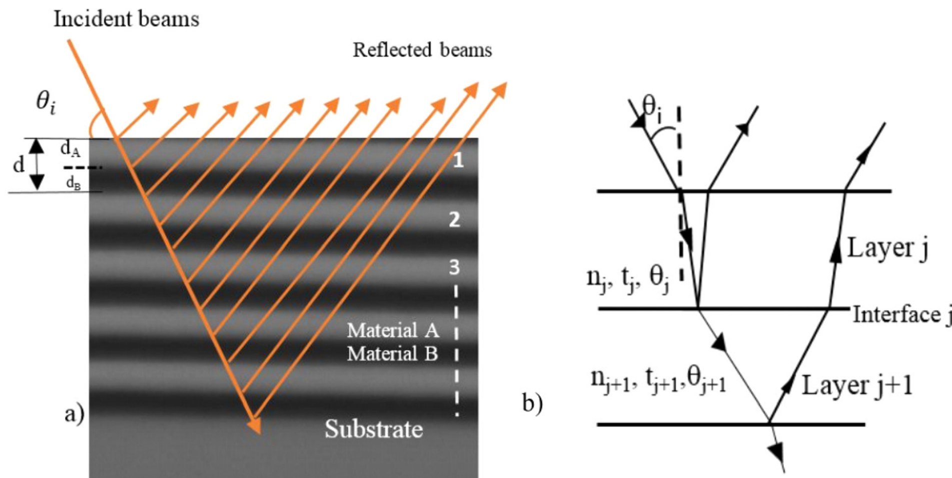

FIG. 1. (a) Schematic of multilayer structure, (b) schematic of EM wave propagation in a ML with incidence angle θ measured from normal at the top layer, and θ_j angle of refraction in the jth layer.[20]

irregularities, where σ is rms roughness and q refers to momentum transfer vector, are chosen for the numerical calculations of reflectivity in IMD.[16] Parratt's method assumes continuity of electric field in the perpendicular direction to the ML.[19] For a generalized multilayer structure shown in Fig. 1 with layer j having thickness t_j and complex refractive index n_j, Fresnel reflection coefficient for *S*-polarized radiation from an interface lying between layers j and $j+1$ is given by

$$r^{s}_{j,j+1} = \frac{n_j \cos\theta_j - n_{j+1}\cos\theta_{j+1}}{n_j \cos\theta_j + n_{j+1}\cos\theta_{j+1}}. \quad (1)$$

In similar manner, Fresnel coefficient for *p*-polarized radiation is calculated in Eq. (2)

$$r^{p}_{j,j+1} = \frac{n_j \cos\theta_{j+1} - n_{j+1}\cos\theta_{j}}{n_j \cos\theta_{j+1} + n_{j+1}\cos\theta_{j}}. \quad (2)$$

Parratt's method calculates the total reflected amplitude ζ_j from the jth interface using a recursive relation (Eq. (3))

$$\zeta_j = \frac{r_{j,j+1} + \chi_{j+1}\exp(-i2\varphi_{j+1})}{1 + r_{j,j+1}\chi_{j+1}\exp(-i2\varphi_{j+1})}, \quad (3)$$

where $\varphi_j = \frac{2\pi}{\lambda} t_j n_j \cos\theta_j$ and χ_{j+1} contains reflectivity contributions from subsequent interfaces. In EUV and soft X-ray wavelengths, the complex refractive index n_j is given by

$$n_j = 1 - \delta_j - i\beta_j, \quad (4)$$

where δ_j and β_j are real values and in the order of $\cong 10^{-3}$ for most elements.

Because Parratt's method assumes semi-infinite substrate thickness, reflection from the bottom structure (i.e., substrate) is zero. Loss of reflectivity due to interfacial roughness and diffuseness can be accounted in Eqs. (1) and (2) by multiplying Fresnel coefficients at each interface by the preferred interface profile functions.

Genetic algorithm (GA) and a more complex form of it known as differential evolution (DE) are alternatively used in the fitting optimization. Detailed description of the GA has been published in Ref. 21. GA is considered as a global optimization algorithm as it is generally less sensitive to the choice of initial parameter values and less susceptible to stacking at local minima even when the function contains more than one peak. In contrast to other methods, GA combines a stochastic search of global minima in a parameter space with intelligent strategy of solution finding.[22] In addition, a manual tuning of parameters to visualize in real time the resulting effect on reflectance was performed based on previous work reported in Ref. 23 to set initial parameters values relatively close to the final values in order to minimize influence of initial parameters on the convergence of the algorithm. Thus, layer and interlayer thicknesses, optical constants, interface diffusion layers, and their stoichiometric compositions are retrieved. To minimize numerical uncertainties due to the number of free parameters, period of MLs as obtained from XRR analysis is adopted in the GI-EUVR fittings. The ML structure (of sample_02 for now) is modeled based on a four-layer system (i.e., layer 1 + interlayer_01 + layer 2 + interlayer_02) to account for interdiffusion regions as independent layers as witnessed from the STEM image. For such ML model, a basic roughness of 2–5 Å suffices to account interface irregularities between interlayers and layers.[24]

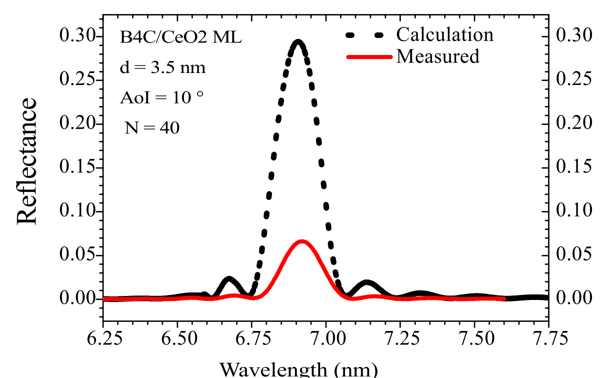

FIG. 2. Calculated and measured reflectivity curves for sample_01. Tabulated values of δ and β available at the Center for X-ray Optics (CXRO) database (http://henke.lbl.gov/optical_constants/) are used for the theoretical calculations. Original vales are determined by Henke and his co-authors as reported in Ref. 25.

Reuse of AIP Publishing content is subject to the terms at: https://publishing.aip.org/authors/rights-and-permissions. IP: 147.162.2.240 On: Tue, 01 Mar 2016 15:38:42

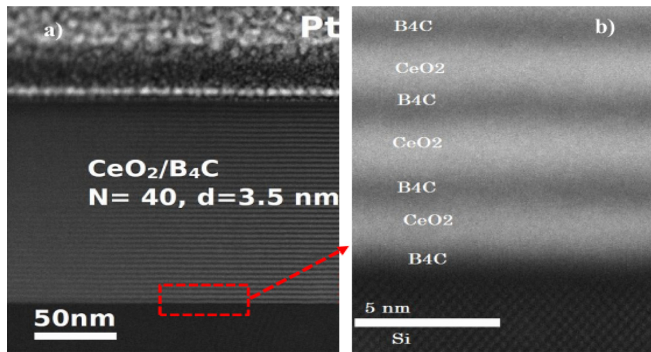

FIG. 3. Atomic resolution of high angle annular dark field (HAADF) image for sample_01. (a) An overview of the ML and (b) atomic resolution of few bilayers near the Si substrate. Note that in HAADF image, brighter spots typically represent the heavier atoms and darker ones represent lighter atomic columns.

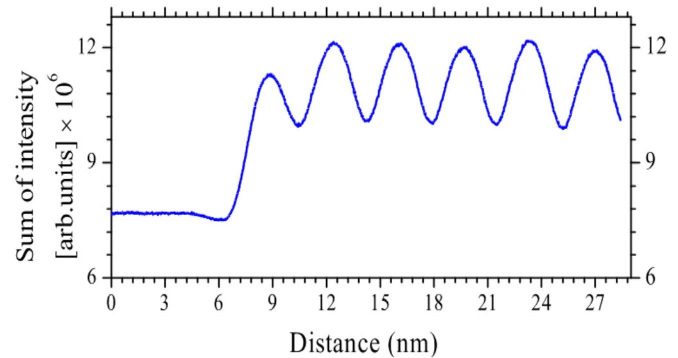

FIG. 5. Sum intensity profile in the [−110] axis of the Si substrate in the HAADF image given in Fig. 4.

III. RESULTS AND DISCUSSION

Measured and calculated EUV reflectivity at 10° from normal for sample_01 is given in Fig. 2.

The measured reflectivity performance at 10° from normal is 6.65%. This is 4.4 times lower than theoretical value. HAADF image of this ML sample (i.e., sample_01) confirms presence of interface diffusion (see Fig. 3) which can be a major cause for the low reflectivity performance.

It is shown that Si atomic columns in the substrate are clearly resolved in the HAADF image (Fig. 3(b)). A more detailed view of the atomic resolution image in the [001] and [−110] axes of the Si substrate is given in Fig. 4. The bottom onset image here shows the inter-diffusions at the interfaces.

Therefore, the HAADF image of sample_01 confirms formation of inter-diffusion layers at the interfaces. Such inter-diffusion regions urged a continuous (contrary to sharp) transition of intensity profile (see Fig. 5) in the [001] axis of the atomic resolution HAADF image given in Fig. 4. It is then obvious that the low reflectivity performance of the ML reported above in Fig. 2 is mainly due to the interface diffusions.

However, further analysis is necessary to explain the physical and chemical properties of the inter-diffusion layers between B_4C and CeO_2 layers for EUV and soft X-ray applications. A method equally sensitive to optical properties as to thickness is required. In fact, approximate thicknesses of layers and interlayer might be derived from the STEM images or from the intensity profiles, but that does not account the influence of optical parameters near the absorption edges of EUV wavelengths in determining the measured reflectivity curves. Due to high sensitivity of atoms to local interactions, actual measurement of optical properties is needed in EUV and soft X-rays in general and near the transition edge energies in particular.

Thus, a systematic combination of X-ray reflectivity and GI-EUVR measurements near absorption edge is performed to derive optical, structural, and morphological properties of the inter-diffusion regions, B_4C and CeO_2. The XRR analysis allows determination of ML period with reasonable accuracy because of its high in-depth resolution at Cu-K_α wavelength (∼1.5 Å) and high sensitivity to Bragg peaks. The at-wavelength GI-EUVR enables derivation of optical constants with high sensitivity, and accounts possible trade-off between thickness and optical parameters in the wide grazing angle measurement setup as explained in Ref. 26.

Here, a grazing incidence at-wavelength reflectivity analysis near EUV absorption edge of the low-Z element (i.e., boron) is performed for sample_02. Sample_02 was fabricated from same materials and in similar deposition conditions (gas pressure, substrate temperature, and ultra-high vacuum properties) as that of sample_01. Thus, interface profiles and optical constants of layers and interlayers

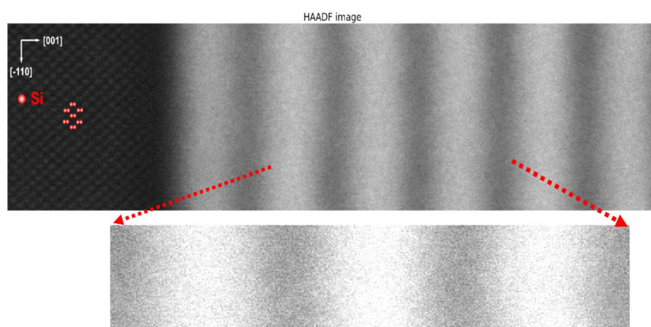

FIG. 4. Atomic resolution of HAADF image showing Si atomic columns in the substrate. The bottom onset image (after little enhancement in contrast) clearly shows the magnitude of inter-diffusion at the interfaces.

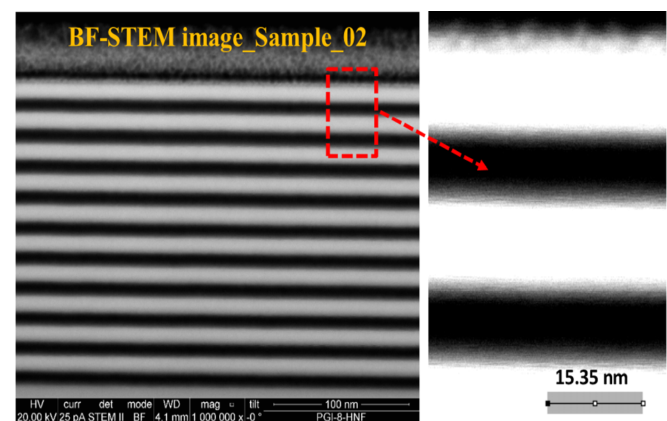

FIG. 6. Bright field-scanning transmission electron microscopy (BF-STEM) image of sample_02. Interface diffusion is clearly visible on the onset image. Int_01 refers to B_4C–on-CeO_2 interfacial diffusion and Int_02 vice versa.

Reuse of AIP Publishing content is subject to the terms at: https://publishing.aip.org/authors/rights-and-permissions. IP: 147.162.2.240 On: Tue, 01 Mar 2016 15:38:42

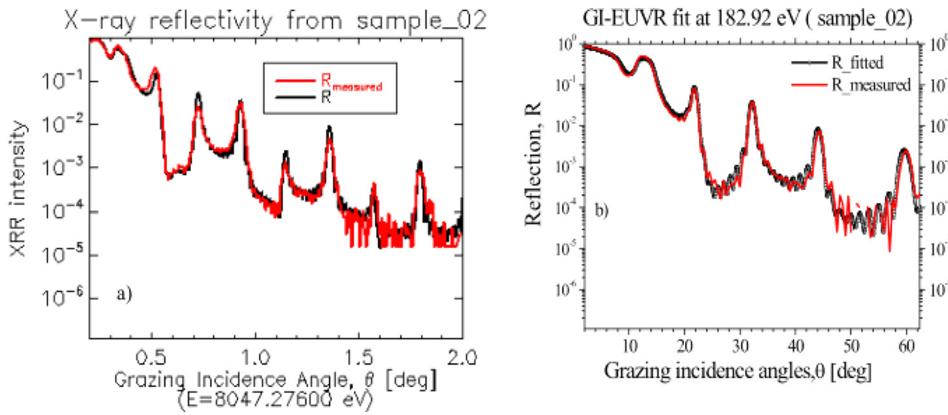

FIG. 7. (a) Nonlinear curve fit to the X-ray data at the Cu K_α line for sample_02. (b) Nonlinear curve fit to the GI-EUVR data at 182.92 eV of sample_02.

derived from sample_02 are representative of sample_01. As mentioned above, a four-layer ML structure (B_4C layer + interlayer 01 + CeO_2 layer + interlayer 02) model that accounts the interface diffusions evidenced from the BF-STEM image of sample_02 (Fig. 6) is implemented during the GI-EUVR data analysis. Interlayer 01 (int_01 in short) and interlayer 02 (int_02) represent the diffusion layers of B_4C-on-CeO_2 and CeO_2-on-B_4C, respectively.

Analysis of the XRR data at the Cu K_α line for sample_02 (Fig. 7(a)) returns period $d = 199.4 \pm 0.11$ Å. GI-EUVR data fit of this sample at 182.92 eV by taking the ML period as obtained from the XRR analysis is shown in Fig. 7(b). Such GI-EUVR analysis of sample_02 is performed for EUV photon energies from 177.53 eV–183.82 eV (slightly below the B-edge). The short range of photon energies is chosen to test the reliability of the analysis method implemented here and then measurements over larger ranges of EUV energies (both above and below the B-edge) will be included in our next work plan.

Optical constants (δ and β) and layer and interlayer thicknesses derived from the fittings of GI-EUVR data, within the confidence intervals in IMD, of sample_02 for different photon energies are summarized in Table II. Note that ML period derived from the XRR analysis is fixed during the GI-EUVR analysis.

For clarity, comparisons with values of δ and β determined by Henke and available at the CXRO database are given in Figs. 8(a) and 8(b) for B_4C and CeO_2 layers, respectively. Measured optical constants clearly demonstrate a strong nonlinear pattern near the absorption edge of boron, unlike the linear behavior of the tabulated values from CXRO database. The optical constants of B_4C layers obtained are also fully consistent with the magnetron sputtered B_4C thin films measured by Soufli *et al.*,[27] Monaco *et al.*,[28] and Ksenzov *et al.*[29]

The change of optical constants of layers in sample_02 as a function of photon energy, as derived from GI-EUVR data analysis, is plotted in Fig. 9. As expected, the optical constants (δ) of int_01 and int_02 shown Fig. 9(a) are bound by that of B_4C from below and CeO_2 from above. The fact that δ values of int_02 (CeO_2–on–B_4C inter-diffusion region) lie far from top and bottom boundaries shows dominance of B_4C atoms, while int_01 (B_4C–on–CeO_2 region) seems to be dominated by CeO_2 atoms. EUV and soft X-ray reflection curves, particularly near the resonance edges, are more critical on δ contrast ($\Delta\delta$) of layers, which makes the accuracy of β values in Fig. 9(b) less accurate and difficult to withdraw any conclusion from it.

Finally, ideal reflectivity performance of sample_01 at incident photon energy E = 183.82 eV is calculated as given in Fig. 10 by using the new optical constants of B_4C and CeO_2 from Table II. Period and thickness ratio of sample_01 are slightly modified to d = 34.80 Å, $\Gamma = 0.43$ in optimizing the reflectivity because of new optical constants used for calculation.

Reflectivity of 35.3% is achieved for an incidence angle of 10° from surface normal. This performance level is significantly higher than the theoretical reflectivity calculated from tabulated optical constants by Henke *et al.* as shown in Fig. 2. This demonstrates that values provided in the available

TABLE II. Sample data within the confidence intervals of sample_02 calculated from combined analysis of XRR and GI-EUVR measured data. In brackets are derived thicknesses from the GI-EUVR analysis, keeping period of the ML fixed as obtained from XRR.

Photon energy (eV)	B_4C_layer (98.1 Å)		Int- 01_layer (18.5 Å)		CeO_2_layer (56.9 Å)		Int 02_layer (25.98 Å)	
	δ	B	δ	β	δ	β	δ	β
177.53	0.005711	0.00111	0.012503	0.002097	0.023407	0.003163	0.022739	0.005449
178.42	0.005294	0.001096	0.012242	0.002560	0.023487	0.003177	0.022682	0.004731
179.32	0.004594	0.001075	0.01320	0.0029633	0.023478	0.003090	0.02190	0.005645
180.22	0.004465	0.00103	0.011591	0.002784	0.023255	0.003387	0.022741	0.0049137
181.12	0.004614	0.00109	0.011854	0.002030	0.022300	0.003008	0.021484	0.005330
182.02	0.003631	0.00103	0.012025	0.002210	0.021832	0.002780	0.021526	0.005850
182.92	0.004078	0.0012182	0.013590	0.001650	0.021211	0.00182	0.019411	0.006110
183.82	0.002703	0.0009512	0.013572	0.005313	0.024804	0.00312	0.022615	0.004774

Reuse of AIP Publishing content is subject to the terms at: https://publishing.aip.org/authors/rights-and-permissions. IP: 147.162.2.240 On: Tue, 01 Mar 2016 15:38:42

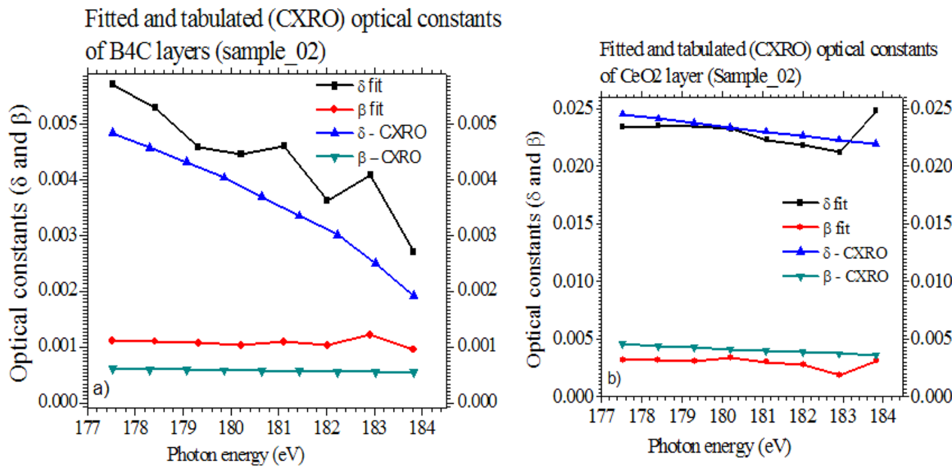

FIG. 8. Optical constants (δ and β) retrieved from the GI-EUVR data fittings and tabulated values from CXRO database. (a) B_4C layer and (b) CeO_2 layer. Note that optical constants of B_4C and CeO_2 are also representative of sample_01.

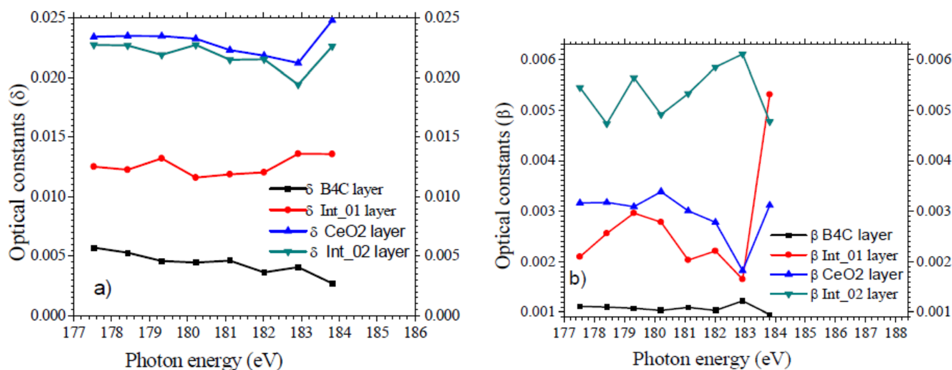

FIG. 9. Graphical summary of calculated optical constants from the XRR and GI-EUVR measured data for sample_02 with (a) δ values and (b) β values. Note that optical constants of B_4C and CeO_2 are also representative of sample_01.

databases may be quite inaccurate for designing new optical coatings. The method of measurements described above can provide a way for improving the much needed knowledge of the optical properties of materials used for advancing the nano-technology.

IV. SUMMARY

Multilayers of B_4C/CeO_2 for below 10 nm EUV applications were fabricated for the first time in a magnetron sputtering facility. Reflectivity performance of the ML (sample_01) at 6.9 nm wavelength and 10° incidence angle from surface normal is determined to be 4.4 times less than

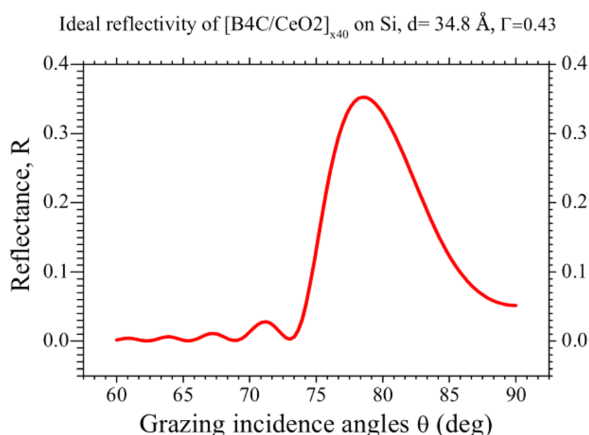

FIG. 10. Ideal reflectivity performance of B_4C/CeO_2 ML with N = 40, d = 34.8 Å, Γ = 0.43 at incident photon energy of 183.82 eV (~6.75 nm).

the theoretical calculations. This performance is in the same scale with the first reported La/B multilayer for the 6.x EUVL application by Makhotkin *et al.*[14] before further optimizations in deposition were taken. As a first attempt to grow such MLs, the result might not be scary but it is a low performance which needs detailed investigation. Therefore, several experimental measurements were performed to understand the major cause for low performance of the ML structures and gaining feedback for future deposition optimizations. GI-EUV reflectivity, X-ray reflection at Cu-K_α, HAADF, BF-STEM imaging, and other relevant measurements were performed to carry out accurate analysis of the MLs.

Accordingly, major cause for the low reflectivity performance of the B_4C/CeO_2 ML is found to be high inter-diffusion between layers as shown in Figs. 3 and 4. For convenience of the GI-EUVR analysis, sample_02 (with thicker period and thus several EUV Bragg peaks) was chosen for the derivation of optical constants of inter-diffusion layers. Asymmetric inter-diffusion layers are found to be formed in a magnetron deposited B_4C/CeO_2 ML with CeO_2-on-B_4C thicker than B_4C-on-CeO_2 (25.98 Å vs 18.5 Å).

Optical constants of layers and interlayers for short range of photon energies (177.53–183.82 eV) near the boron edge are derived. The δ and β of B_4C are consistent with previously reported measurements by Soufli *et al.*[27] and Ksenzo.[29] It is also worth mentioning that optical constants of CeO_2 layers in the EUV energy range of 177.53–183.82 eV are for the first time measured here. Comparison of optical constants of B_4C and CeO_2 layers with corresponding tabulated values in the CXRO database (originally determined by Henke

Reuse of AIP Publishing content is subject to the terms at: https://publishing.aip.org/authors/rights-and-permissions. IP: 147.162.2.240 On: Tue, 01 Mar 2016 15:38:42

et al.) show abrupt variation of the currently measured optical constants unlike the linear behavior in the tabulated ones. This is likely due to the higher sensitivity of near edge EUV optical constants to influences of fine structure.

Finally, ideal reflectivity performance of the B_4C/CeO_2 combination based on optical constants derived using the current analysis is found to be significantly higher than what was calculated theoretically from the tabulated values. This demonstrates that values provided in the available databases may be quite inaccurate for designing new optical coatings.

ACKNOWLEDGMENTS

We acknowledge financial support from the EU FP7 Erasmus Mundus Joint Doctorate Program EXTATIC under framework partnership Agreement No. FPA-2012-0033. We also thank Dr. Elmar Neumann of the PGI-8-PT group in the Forschungszentrum Jülich for making the STEM images. Thanks to the ELETTRA Synchrotron that financed the work under Proposal No. 20140313 to make experiments at the BEAR beam line. This work was also performed under the support of STSM COST Action MP1203. Special gratitude to P. Zuppella, A. J. Corso, and A. Maryasov for helpful discussions. Finally, we thank David L. Windt for making available the latest version of IMD software (version 5.04).

[1]B. Kneer, S. Migura, W. Kaiser, J. T. Neumann, and J. van Schoot, in *Extreme Ultraviolet*, edited by O. R. Wood and E. M. Panning (Proc. SPIE, Extreme Ultraviolet (EUV) Lithography VI, 2015), Vol. 9422.
[2]T. S. Kulmala, M. Vockenhuber, E. Buitrago, R. Fallica, and Y. Ekinci, in *Extreme Ultraviolet*, edited by O. R. Wood and E. M. Panning (Proc. SPIE, Extreme Ultraviolet (EUV) Lithography VI, 2015), Vol. 9422.
[3]M. G. Sertsu, A. Giglia, S. Brose, A. Comisso, Z. S. Wang, L. Juschkin, and P. Nicolosi, in *EUV and X-Ray Optics: Synergy Between Laboratory and Space IV*, edited by R. Hudec and L. Pina (Proc. SPIE, EUV and X-ray Optics: Synergy between Laboratory and Space IV, 2015), Vol. 9510.
[4]N. I. Chkhalo, M. N. Drozdov, E. B. Kluenkov, A. Y. Lopatin, V. I. Luchin, N. N. Salashchenko, N. N. Tsybin, L. A. Sjmaenok, V. E. Banine, and A. M. Yakunin, J. Micro/Nanolithogr. MEMS MOEMS **11**(2), 021115 (2012).
[5]T. Otsuka, D. Kilbane, T. Higashiguchi, N. Yugami, T. Yatagai, W. Jiang, A. Endo, P. Dunne, and G. O'Sullivan, Appl. Phys. Lett. **97**(23), 231503 (2010).
[6]S. L. Nyabero, R. W. van de Kruijs, A. E. Yakshin, I. A. Makhotkin, J. Bosgra, and F. Bijkerk, J. Micro/Nanolithogr. MEMS MOEMS **13**(1), 013014 (2014).
[7]S. N. Yakunin, I. A. Makhotkin, K. V. Nikolaev, R. W. E. van de Kruijs, M. A. Chuev, and F. Bijkerk, Opt. Express **22**(17), 20076–20086 (2014).
[8]I. A. Makhotkin, E. Zoethout, E. Louis, A. M. Yakunin, S. Mullender, and F. Bijkerk, Opt. Express **20**(11), 11778–11786 (2012).
[9]P. Naujok, S. Yulin, A. Bianco, N. Mahne, N. Kaiser, and A. Tuennermann, Opt. Express **23**(4), 4289–4295 (2015).
[10]S. Andreev, M. Barysheva, N. Chkhalo, S. Gusev, A. Pestov, V. Polkovnikov, N. Salashchenko, L. Shmaenok, Y. A. Vainer, and S. Y. Zuev, Nucl. Instrum. Methods Phys. Res., Sect. A **603**(1), 80–82 (2009).
[11]Y. Platonov, J. Rodriguez, M. Kriese, E. Gullikson, T. Harada, T. Watanabe, and H. Kinoshita, "the SPIE optics + optoelectronics," Proc. SPIE **8076**, 80760N (2011).
[12]D. Kuznetsov, A. Yakshin, J. Sturm, R. van de Kruijs, E. Louis, and F. Bijkerk, Opt. Lett. **40**(16), 3778–3781 (2015).
[13]N. Chkhalo, S. Künstner, V. Polkovnikov, N. Salashchenko, F. Schäfers, and S. Starikov, Appl. Phys. Lett. **102**(1), 011602 (2013).
[14]I. A. Makhotkin, E. Zoethout, R. van de Kruijs, S. N. Yakunin, E. Louis, A. M. Yakunin, V. Banine, S. Mullender, and F. Bijkerk, Opt. Express **21**(24), 29894–29904 (2013).
[15]S. Nannarone, F. Borgatti, A. DeLuisa, B. P. Doyle, G. C. Gazzadi, A. Giglia, P. Finetti, N. Mahne, L. Pasquali, M. Pedio, G. Selvaggi, G. Naletto, M. G. Pelizzo, and G. Tondello, in *Synchrotron Radiation Instrumentation*, edited by T. Warwick, J. Arthur, H. A. Padmore, and J. Stohr (AIP Conf. Proc., 2004), Vol. 705, pp. 450–453.
[16]D. L. Windt, Comput. Phys. **12**(4), 360–370 (1998).
[17]M. Lampton, B. Margon, and S. Bowyer, Astrophys. J. **208**(1), 177–190 (1976).
[18]T. Yaqoob, Astrophys. J. **500**(2), 893–898 (1998).
[19]Y. Chung-Jong, K. Euikwoun, and K. Jae-Yong, J. Nanosci. Nanotechnol. **11**(5), 4624–4628 (2011).
[20]R. Jirawit, "Design and fabrication of Aperiodic multilayers with broad-band reflectance in the Soft X-ray regime," University of Cambridge, 2014.
[21]P. D. Binda and F. E. Zocchi, in *Advances in Computational Methods for X-Ray and Neutron Optics*, edited by M. S. DelRio (SPIE, Bellingham, WA, 2004), Vol. 5536, pp. 97–108.
[22]A. Ulyanenkov, K. Omote, and J. Harada, Physica B **283**(1–3), 237–241 (2000).
[23]S. M. Giday, P. Zuppella, M. G. Pelizzo, and P. Nicolosi, "the optics for EUV, x-ray, and gamma-ray astronomy VI," Proc. SPIE **8861**, 886111 (2013).
[24]J. Serafinczuk, J. Pietrucha, G. Schroeder, and T. P. Gotszalk, Opt. Appl. **41**(2), 315–322 (2011).
[25]B. L. Henke, E. M. Gullikson, and J. C. Davis, At. Data Nucl. Data Tables **54**(2), 181–342 (1993).
[26]M. G. Sertsu, M. Nardello, A. Giglia, A. J. Corso, C. Maurizio, L. Juschkin, and P. Nicolosi, Appl. Opt. **54**(35), 10351–10358 (2015).
[27]R. Soufli, A. L. Aquila, F. Salmassi, M. Fernandez-Perea, and E. M. Gullikson, Appl. Opt. **47**(25), 4633–4639 (2008).
[28]G. Monaco, D. Garoli, R. Frison, V. Mattarello, P. Nicolosi, M. Pelizzo, V. Rigato, L. Armelao, A. Giglia, and S. Nannarone, "the SPIE optics+photonics," Proc. SPIE **6317**, 631712 (2006).
[29]D. Ksenzov, T. Panzner, C. Schlemper, C. Morawe, and U. Pietsch, Appl. Opt. **48**(35), 6684–6691 (2009).

Reuse of AIP Publishing content is subject to the terms at: https://publishing.aip.org/authors/rights-and-permissions. IP: 147.162.2.240 On: Tue, 01 Mar 2016 15:38:42